UNCONVENTIONAL MICROFABRICATION USING POLYMERS

A Thesis Presented to

The Academic Faculty

By

Andrew Hampton Cannon

In Partial Fulfillment of the Requirements for the Degree

Master of Science in Mechanical Engineering

Georgia Institute of Technology

December 2006

UNCONVENTIONAL MICROFABRICATION USING POLYMERS

Approved:

Dr. William P. King, Chair
Mechanical Engineering
Georgia Institute of Technology

Dr. Samuel Graham
Mechanical Engineering
Georgia Institute of Technology

Dr. Clifford L. Henderson
Chemical and Biomolecular Engineering
Georgia Institute of Technology

Date Approved: 8/28/2006

ACKNOWLEDGEMENTS

I would like to thank my thesis advisor, Dr. William P. King, for giving me the support I needed to work creatively on a wide range of research projects. I also thank Dr. Samuel Graham and Dr. Clifford L. Henderson for working with me and providing me with lab support on the projects described in this thesis. Yueming Hua and Ashanté Allen were also integral parts of the projects described in this thesis.

I also thank my fellow graduate students who provided assistance to me

TABLE OF CONTENTS

LIST OF FIGURES

SUMMARY

Current microfabrication materials include silicon, a wide variety of metals, dielectrics, and some polymers [1-4]. Because of the low cost and high processing flexibility that polymers generally have, expanding the use of polymers in microfabrication would benefit the microfabrication community [1, 5-7], enabling new routes towards goals such as low-cost 3D microfabrication.

This work describes two main unconventional uses of polymers in microfabrication. The first unconventional use is as a carrier material in the self-assembly (SA) of millimeter-scale parts in which functional electronic components and electrical interconnects were cast into 5 mm cubes of Polymethylmethacrylate (PMMA) [8]. The second unconventional use is as a non-flat micromold for an alumina ceramic and as transfer material for multiple layers of micropatterned carbon nanotubes (CNTs). Both of these uses demonstrate 3D low-cost microfabrication routes.

In the SA chapter, surface forces induced both gross and fine alignment of the PMMA cubes. The cubes were bonded using low-melting temperature solder, resulting in a self-assembled 3D circuit of LEDs and capacitors. The PMMA-encasulated parts were immersed in methyl methacrylate (MMA) to dissolve the PMMA, showing the possibility of using MEMS devices with moving parts such as mechanical actuators or resonators. This technique could be expanded for assembly of systems having more than 10^4 components. The ultimate goal is to combine a large number of diverse active components to allow the manufacture of systems having dense integrated functionality.

The ceramic micromolding chapter explores micromolding fabrication of alumina ceramic microstructures on flat and curved surfaces, transfer of carbon nanotube (CNT) micropatterns into the ceramic, and oxidation inhibition of these CNTs through ceramic encapsulation. Microstructured master mold templates were fabricated from etched silicon, embossed thermally sacrificial polymer, and flexible polydimethylsiloxane (PDMS). The polymer templates were themselves made from silicon masters. Thus, once the master is produced, no further access to a microfabrication facility is required. Using the flexible PDMS molds, ceramic structures with mm-scale curvature were fabricated having microstructures on either the inside or outside of the curved macrostructure. It was possible to embed CNTs into the ceramic microstructures. To do this, micropatterned CNTs on silicon were transferred to ceramic via vacuum molding. Multilayered micropatterned CNT-ceramic devices were fabricated, and CNT electrical traces were encapsulated with ceramic to inhibit oxidation. During oxidation trials, encapsulated CNT traces showed an increase in resistance that was 62% less than those that were not encapsulated. The processes described here could allow fabrication of inexpensive 3D ceramic microstructures suitable for high temperature and harsh chemical environments.

CHAPTER 1

INTRODUCTION

1.1 Motivation for Research

Materials currently used in microfabrication include silicon, metals, dielectrics, and some polymers [1-4]. Because of the low cost and high process flexibility that polymers generally have, expanding the use of polymers in microfabrication beyond patterning and encapsulation of devices would benefit the microfabrication community [1, 5-7]. The self-assembly of functional devices and ceramic micromolding are two areas where using polymers can lower the cost of manufacturing and allow new manufacturing techniques that build devices in 3D.

Self-Assembly (SA) is a parallel manufacturing technique where structures of any size organize according to a highly preferential thermodynamic configuration, seemingly self-directed. SA has advantages over pick-and-place methods for microelectronics assembly that require independent manipulation of each component and are inherently 2D, in that SA is parallel and amenable to 3D assembly. As such, it is well-suited to heterogeneous 3D integration of next-generation Microsystems [9-13]. Because of its nanoscale to mesoscale range, 3D nature and speed through parallel assembly, SA has the potential to improve sensors integration and assembly [13, 14], enable the prototyping and manufacture of hybrid systems formed of novel and diverse materials [15, 16], and allow prototyping and manufacture of complex systems built from microscaled templates

[9]. Using polymer as a sacrificial carrier material for functional devices, components can be self-assembled and then exposed to the environment by dissolving the polymer.

SA relies on configurational energy minimization, where components are agitated or experience Brownian motion sufficient to test a number of possible configurations. Once the components reach an arrangement that has minimal configurational energy, the system is stable or quasi-stable. Figure 2 shows an unstable system in configuration A. Brownian motion or agitation will cause the system to move towards configuration B, the minimum system free energy. A system in configuration C is at a local minimum and is quasi-stable. Sufficient activation energy must be supplied to move the system over the energy barrier to configuration D, the global minimum. Predetermined self-assembled configurations can be created by tailoring system energetics towards a target configuration.

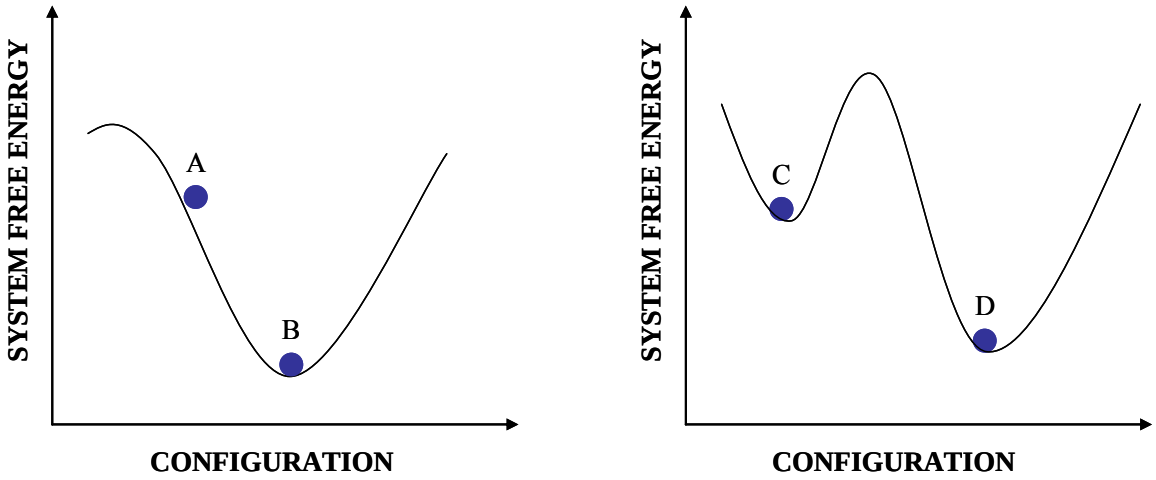

Figure 1. Thermodynamic System Free Energy VS. System Configuration

Two types of self-assembly have been demonstrated for small parts, the main distinction being the presence of liquid water or a liquid-environment interface. Figure 2

shows these two types of SA. The most common method of SA is to use capillary forces at a liquid-air, solder-water, or adhesive-water interface to promote the SA and self-alignment of 2D microparts and 3D polyhedra [9-11, 13, 17, 18]. The driving force of self-alignment is the minimization of the capillary-environment interfacial energy. Initially, separate parts have curved solder-liquid interfaces. When the solder-liquid interfaces initially meet and join, the overall interfacial surface area decreases, lowering the overall surface energy which lowers the system free energy. The system free energy continues to decrease because of the decreasing capillary-environment interfacial surface area, aligning the parts until a minimum in the interfacial surface area curve has been met. Capillary forces can be used to cause SA from the mesoscale to the nanometer-scale [9, 12, 19], and have been used to align micro surface features to sub-micron accuracy [3, 9, 11, 14]. Figure 2A shows two flat parts that have been brought together by capillary forces. Originally the top and bottom parts were separate with a fixed water-air interfacial energy. When the water-air interfaces touched, a lower interfacial energy became possible, driving the capillaries to minimize the interfacial surface area with the environment because of minimization of the system free energy. A less common method for SA is to allow hydrophobic surfaces to exclude water, bringing the self-aligning surfaces into full contact [19], as shown in Figure 2B. Nanometer-scale SA is also possible by use of weak ionic bonds, hydrogen bonds, and van der Waals interactions [20].

A. Capillary Force-Induced Alignment of Micro Surface Features

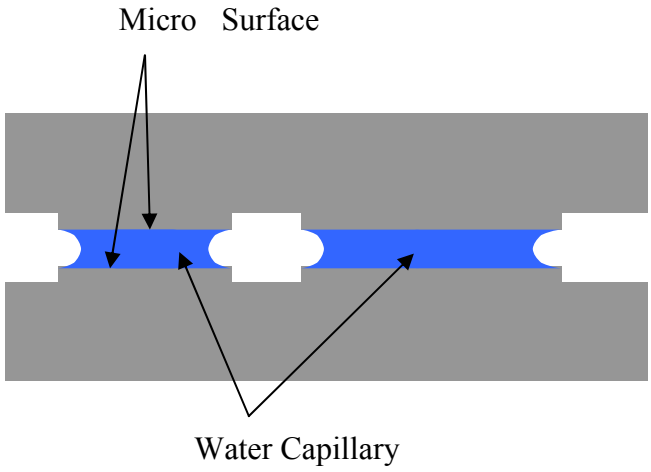

B. Hydrophobic Force-Induced Alignment of Micro Surface Features

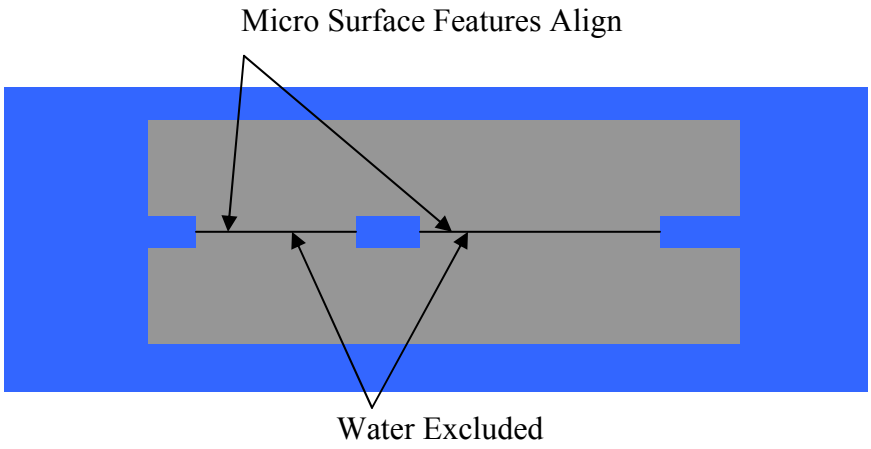

Figure 2. A) Capillary Force Alignment of Micro Surface Features. B) Hydrophobic Force Alignment of Micro Surface Features

Several recent reports describe 2D SA of homogeneous micrometer- and millimeter-sized parts. Fluidic SA of micron-sized silicon parts onto silicon and quartz substrates was performed using heat-activated and photocurable methacrylate lubricant-adhesives for capillary force-driven SA and bonding in water [21]. An alignment accuracy of better than 0.2 μm was achieved for 98-part arrays in less than 1 minute and

100% yield. Another technique that used capillary forces caused SA of 113 GaAlAs LEDs with a chip size of 280 μm onto a cylindrical display, and 1500 silicon cubes self-assembled on 5 square centimeters in less than 3 minutes with a defect rate of 2% [22]. 2D templates that determine the final structure of self-assembled components were also developed, dictating the 2D macro-structure of flat parts and enabling greater control of the final system arrangement [9]. Another technique that used lubricant-adhesives for capillary force-driven SA made possible the sequential assembly of multiple batches of micro-components onto a single substrate by using alternating hydrophobic and hydrophilic binding sites to activate specific binding sites [13, 23]. The lubricant-adhesive only wetted the hydrophobic sites, thereby dictating the sites where SA occurred. After chemically changing the remaining hydrophilic sites to be hydrophobic, another batch of components self-assembled on the new lubricant-adhesive binding sites. Mathematical models of capillary forces have been developed that describe the effect of a variety of geometries' area overlap [24] and how a single part may react to being twisted, tilted, shifted, and lifted [25]. As the capillary becomes thinner, its restoring force to its system free energy minimum becomes stronger. Capillary force-driven SA cannot be used to uniquely orient parts with binding sites that are rotationally symmetric. A peg-in-hole and gravity driven self-alignment technique addressed the symmetry issue and resulted in 98%-yield wafer-level packaging for micro devices using uniquely orienting self-assembling 2 mm square diced silicon parts. Each silicon part had one hydrophobic thiolated gold face and one circular peg, offset from the center of mass, on the opposite face. A receptor site on an alignment template had a circular trap hole [26]. A SA process that assembled sub-millimeter micro-electro-mechanical-systems (MEMS) chips

in air addressed problems related to fluidic SA such as stiction for released MEMS chips. Components were agitated on a vibrating diaphragm and captured via capillary forces on a substrate with downward facing binding sites [27]. The components self-assembled at a rate of 0.125 components/sec·site with a yield of 93%. The further development of 2D SA could enable low cost, high speed alternatives to expensive pick-and-place techniques that are serial in nature.

SA can be used to give 3D functionality to surface micro-machined MEMS and to enable the manufacture of densely packed electronics. The solder-air interface has been used for the SA of multiple joint solder self-assembled MEMS such as micro-sized axial flow fans and micro cable grippers [28]. Solder was deposited on metal pads on polysilicon hinges. When the solder was heated to reflow, minimization of the solder-air interfacial energy caused the hinge to bend upwards, transforming the previously 2D micropart into a 3D device. Precision of assembly was affected from greatest to least impact by solder volume, solder adherence to metal pads, residual stress in bilayer structures, temperature, structure dimension, solder pad warpage, hinge displacement, and residual stress in single layer structures. In order to demonstrate the feasibility of creating self-assembled 3D electronics, 3D mesoscale homogeneous polyhedra have been self-assembled into macrocrystalline structures using the capillary forces of a low-melting temperature alloy. A functional 3D circuit was formed by mounting LEDs on the surface of the polyhedra. To miniaturize the polyhedra, self-folding structures with 100-300 micron sides were fabricated [15, 17, 29]. Future generations of these structures could be developed into densely packed, 3D electrical networks once challenges with heterogeneity have been overcome. A 3D lock-and-key bonding geometry and sequential

SA was recently used to perform defect-free SA of 600 200 micron-sided LEDs on a 2D silicon substrate [30-33]. The LEDs were then packaged with self-assembled encapsulation units. The 3D lock-and-key technique is one strategy which could enable the SA of heterogeneous 3D microsystems.

Previous research on SA has either used planar micromachined components or homogeneous 3D components. While 3D components have offered potential for substantially higher complexity of the assembled system, the parts for 3D assembly have been nearly identical for any given system. This thesis describes a SA manufacturing technique that allows for the SA of heterogeneous 3D parts to form 3D macrocrystalline structures. Unlike previous published reports on SA, this thesis reports SA of parts having a variety of functions and assembled into a 3D structure, which is enabled through a standard interconnect. By developing an approach for 3D SA of components have different functions, this research improves the function density of SA-manufactured systems.

In addition to polymers being an attractive material for unconventional packaging techniques, they are also can be effectively used for ceramic micromolding. Ceramics are an attractive material for microelectromechanical systems (MEMS) devices because of their robustness at in high temperature, hardness, functional properties, and chemical resistivity [1, 34-36]. Liquid and colloidal suspension precursor-based approaches to ceramic molding make ceramic processing low-cost and flexible to manufacturing needs. Ceramic microdevices could be deployed in harsh environments where silicon is not practical since silicon is not a structural material, chemically resistive, nor a high temperature material. Silicon softens at 600 ºC and reacts with oxygen and water [1]

while alumina, tin oxide, silicon carbide, and borosilicon carbonitride based ceramics can withstand temperatures > 1400 ºC and harsh chemical environments [2, 4, 34, 35, 37-39].

Carbon nanotubes (CNTs) are also an attractive material for MEMS devices because of their low resistivity, high heat capacity, high heat conductance, and a Young's modulus much larger than steel [40-42]. CNTs have been used in plasma devices to reduce power consumption [43, 44] and commercially available CNT-based memory that is faster than traditional computer memory [45].

Recent work on ceramic micromolding has utilized serial and parallel processing techniques to produce 2D and 3D microstructures, almost exclusively on flat surfaces [1, 2, 4, 5, 34, 35, 38, 39, 46-49]. Ceramic micromolding methods have not been developed that produce microstructures on curved surfaces. A technique that used parallel processes to create 2D microstructures was the combination of conventional photolithography with microtransfer molding and vacuum assisted micromolding in capillaries (MIMIC) [4]. This technique produced a borosilicon carbonitride (SiBNC) ceramic honeycomb mesh with 20 μm features that was molded into polydimethylsiloxane (PDMS). The SiBNC ceramic had a 30% linear shrinkage which could cause low molding fidelity. PDMS molds for the ceramic honeycomb microstructures were peeled off the ceramic when possible, and a lost mold technique was employed when mechanical release was not possible. The lost mold technique used a room temperature solution of 1.0 M tetrabutylammonium fluoride in tetrahydrofuran to dissolve the PDMS mold. While this technique produced high-quality 2D microstructures on a flat surface, it did require corrosive chemicals. Another lost mold technique that used corrosive chemicals dissolved microinjection-molded PMMA with methylene chloride [2]. Epoxy-based

metallic or ceramic nanoparticulate slurries were cast into the PMMA micromolds by capillary-driven flow to produce microgears with features of 50 μm.

A lost mold technique that avoided harsh chemicals used heat to thermally decompose a photolighographically patterned SU8 photoresist mold [1]. The possibility for multi-layered ceramic devices was also mentioned. Another thermal decomposition technique used a commercially available sacrificial polymer made from polynorbornene with the trade name Promerus Unity polymer (PUP) and a polymer overcoat layer to package MEMS gyroscopes and accelerometers [5]. When heated, the PUP decomposed into only gaseous by-products and left the MEMS devices sufficiently clean for moving parts to operate. Thermal decomposition avoids the need for corrosive chemicals, but using standard microfabrication equipment makes the molds expensive.

To reduce the expense of photolithography, it is possible to micropattern thermally decomposable polymer via embossing [50]. Embossing as a micropatterning technique is an inexpensive, high-throughput process which reduces the use of microfabrication equipment [6, 7, 51]. Although high throughput processing is attractive, a general disadvantage of thermal decomposition techniques is that if the photoresist and ceramic are both organic, they can react with each other during the high temperature ceramic curing/polymer decomposition process [1].

Microstereolithography is an alternative to lost mold techniques that has produced 3D parts of alumina ceramic [38]. The minimum layer thickness achievable was 20 μm, and the technique produced a wall 60 μm wide and 200 μm tall. While 3D microstructures have great potential for MEMS devices, stereolithography is a serial process, and a minimum layer thickness of 20 μm restricts the construction of the

smallest microstructures [38]. However, a benefit of stereolithography is that it is a good process for rapid prototyping. To prototype ceramic microreactors, stereolithography combined with low-pressure ceramic injection molding has produced a reactor with sub-millimeter components as shown in Figure 3 [34]. The linear shrinkage of the alumina-paraffin wax ceramic precursor used was 12%. The low chemical reactivity and high temperature ability of ceramic make it an ideal material to use in devices such as small-scale reactors. A gas sensor is another device which would benefit from the properties of ceramic. The combination of photolithography and MIMIC with ceramic suspensions has produced a thick-film gas-sensing device based on tin oxide [36]. Gas sensing elements were produced that covered an area of only 10x40 μm or approximately 50 times smaller than what is in present usage. A microturbine is yet another device that would benefit from the high temperature use and low chemical reactivity of ceramic. Stereolithography produced multiple layers of a turbine mold with curved 0.3 mm structures of silicon nitride [46, 49]. Turbines such as these could be a compact way to generate power for devices that require 10-100 W [48].

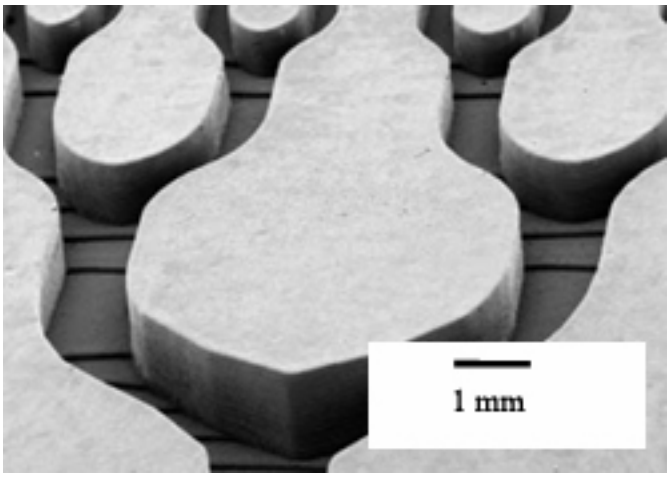

Figure 3. Ceramic reactor fabricated with Microstereolithography combined with low-pressure ceramic injection molding [34]

Some of these techniques used corrosive chemicals and produced microstructures on flat surfaces, others used thermally sacrificial molds produced by photolithography, and still others produced larger 3D microstructures with serial processing techniques. Ceramic micromolding methods have not been developed that produce curved microstructures using parallel processing techniques.

In the present work, etched silicon, embossed thermally decomposable polymer, and flexible PDMS were used as molds for ceramic microstructures using a low-shrinkage alumina-based ceramic precursor [52]. The precursor had an exceptionally low linear shrinkage of 0.1% compared with recent work that used ceramic precursors with a linear shrinkage of 12-30% [2, 4, 34]. The molding techniques avoid the use of corrosive chemicals, use parallel processing techniques rather than serial, employ the use of embossed sacrificial molds, and produce curved macrostructures which incorporate micropatterns on the inside and outside of the macrostructure.

Recently, it has been reported that CNT micropatterns have been transferred to polymer and mixed into rubber and ceramic [53-61]. Microtraces of CNTs have been transferred to flexible PMMA via hot embossing [53, 55] and flexible PDMS via vacuum molding [57], allowing the combination of flexible electronics and CNTs. CNTs have also been mixed into rubber to enhance the Young's modulus of the rubber [54]. CNTs have been mixed into ceramic precursors in order to increase the Young's modulus and electrical conductivity [58-61], and ceramics have been uniformly coated with CNTs [56]. Although CNTs have been incorporated into ceramic for the purpose of enhancing

the bulk mechanical and electrical properties, no work has reported micropatterning of CNTs into the ceramic.

This thesis describes a technique for transferring a 1 cm^2 area of 10 μm wide CNT traces to ceramic and making multilayer CNT-ceramic devices. Because temperatures above ~700 ºC oxidize CNTs and thus mitigate their properties [62], ceramic was used to encapsulate CNT micropatterns. Oxidation trials showed that the ceramic encapsulation inhibited oxidation of the CNTs under high temperature.

1.2 Thesis Overview

The purpose of this research is to introduce new microfabrication methods which use polymers, expanding the microfabrication toolbox to include more low-cost methods. The main properties of polymers which this work utilizes are its ability to be sacrificed after functioning as a carrier material and its flexibility.

Chapter 2 presents work performed on new SA processes and results from those processes. New ceramic micromolding processes and their results are discussed in chapter 3. Chapter 4 discusses conclusions and the direction of future work.

CHAPTER 2

SELF-ASSEMBLY FOR THREE-DIMENSIONAL INTEGRATION OF FUNCTIONAL ELECTRICAL COMPONENTS

The basic strategy of the present packaging method was to embed electronics components into plastic cubes that will self-assemble and bond in solution. The manufacture and packaging of a standard interconnect was first explored, followed by electronics integration.

The first step in pursuing the above goals was developing a technique that allowed carrier structures for functional devices to self-assemble. Capillary forces of a low-melting temperature solder were used to assemble, align, and bond the carrier structures. The next step was casting small electrical components into the carrier structures and self-assembling them into a functional electrical circuit. In the present work, capacitors and LEDs were used. Each capacitor and each LED use 2 sides of their 6-sided carrier structures.

2.1 Fabrication of a Standard Electrical Interconnect Via Self-Assembly

Millimeter-scale carrier structures and standard interconnect were created from Polymethylmethacrylate (PMMA) cubes, copper tape, and a low-melting temperature solder. Figure 4A shows the fabrication process for the carrier structures. A 5 mm-thick sheet of PMMA was cut into 5 mm cubes using a CO_2 laser cutting tool. 80 μm thick copper tape was wrapped around the cubes in a cross pattern. Zinc Chloride solder flux

was applied to the copper, and a solder [63] with melting temperature 47 ºC was brought to 95 ºC to wet the copper. The solder was chosen because it has a melting temperature low enough to be used in water, wets fluxed copper at a temperature substantially below the glass transition temperature of the PMMA carrier pieces, and has an interfacial energy with aqueous KBr that is high enough to cause SA. After wetting the copper with the solder, the cubes were stirred in a 50 ºC aqueous solution of 23% wt. Potassium Bromide (KBr). Minimization of the interfacial energy of the liquid solder with the aqueous KBr caused the carrier structures to self-assemble. The bath was cooled to room temperature, and the carrier structures bonded together. Depending on the particular application, removal of the carrier polymer structure may be desirable. In this work, the resulting macro-structure was immersed in chloroform for six hours to remove the PMMA without damaging the metals' structural integrity. Initial experiments were performed with cross-linked PMMA which swelled rather than dissolved when immersed in chloroform, damaging the copper-solder interconnect. PMMA which was not cross-linked was then used and dissolved easily. The carrier structures took approximately 10 minutes to assemble. As the structures were stirred and shaken, the system moved through different configurations, some being quasi-stable which required more time and agitation to reconfigure. After 10 minutes, capillary forces of the liquid solder caused full alignment of the interconnect. Figure 4B explains the mechanism of alignment. When two curved solder/aqueous KBr interfaces touched, a lower interfacial energy than with the aqueous KBr was reached. The area of the solder/aqueous KBr interface decreased until the system free energy was minimized as described in Figure 2, bringing the structures together for bonding upon cooling. Figure 5 shows the 2x2x3 array of self-assembled

carrier structures. Hand-placement of the copper accounts for the loose macro-structure. Figure 6 shows the same macro-structure from Figure 5 after dissolving the PMMA in chloroform for six hours. When electronics have been embedded in the carrier structures, dissolving the PMMA will allow the use of electronics with moving parts such as actuators and MEMS devices such as gyroscopes and accelerometers.

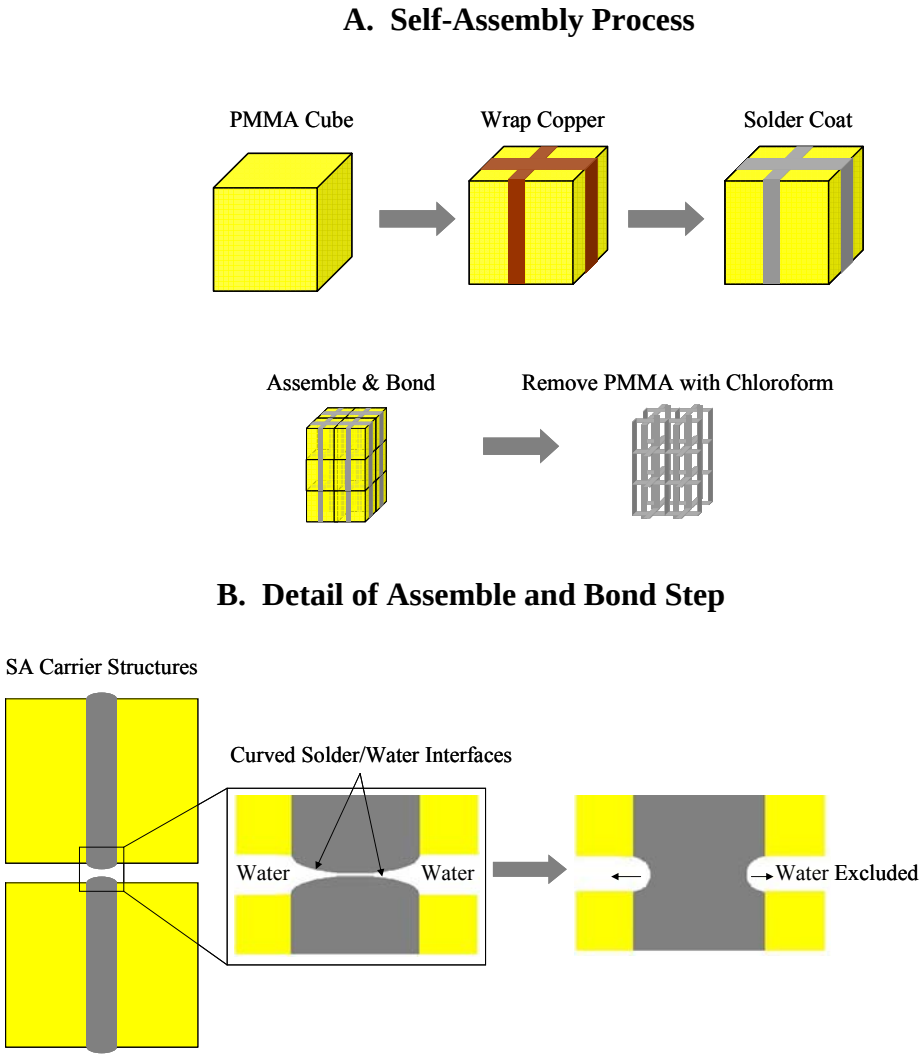

Figure 4. A) Method for Manufacture of Modular Self-Assembly Carrier Structures and Final Macro-Structure: A PMMA cube is wrapped with copper tape, the copper tape is coated with low-melting temperature solder, cubes are self-assembled and bonded, and the PMMA is coated with low-melting temperature solder.

Figure 5. 2x2x3 Array of 5mm-Sided Cube Self-Assembled Carrier Structures

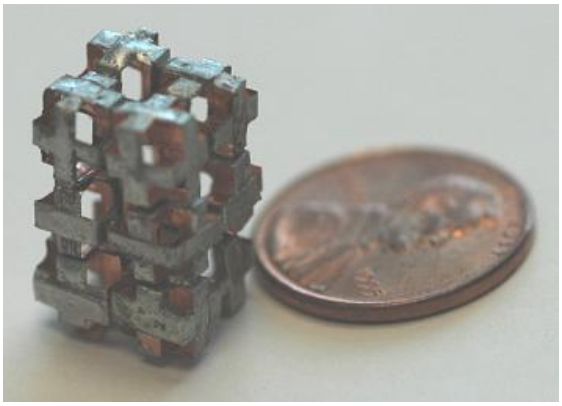

Figure 6. Interconnect Structure from Figure 5 with PMMA Dissolved by Chloroform

2.2 Electronics Integration and Self-Assembly

Having developed a standard interconnect, it was possible to integrate and connect any electrical component that could be encapsulated in carrier structures. Figure 7 shows the strategy for incorporating small parts into the carrier structures. Components were encapsulated in PMMA, copper tape was used as an interconnect, the copper was fluxed and wetted with solder, and the cubes were then stirred in a 50 ºC aqueous solution of 23% wt. KBr. By carrying out the same basic steps shown in Figure 4A, a system of

modular, heterogeneous, 3D, self-assembled components was created. Figure 8 shows the specific manufacturing strategy for incorporating small parts into the carrier structures. Beginning with a mold, copper tape was laid down as an interconnect. Millimeter-scale LEDs and capacitors were placed inside the mold and soldered to the copper tape. PMMA monomer was polymerized in a two-stage process. To make a viscous PMMA fluid which would not seep through the cracks of the mold, the PMMA monomer was heated to 75 ºC for 45 minutes and then used to fill the mold. It was then heated to 55 ºC for 9 hours for full polymerization. A variety of polymers can be used in a similar manner to encapsulate devices and make them suitable for the SA process. Furthermore, many polymers would also be amenable to future selective removal by dissolution. Other mechanisms for selective removal of the polymer are also possible in cases where dissolution in liquid environments are less desirable. For example, polymers which can directly decompose cleanly to gaseous products through heating may be adapted to such applications. The polymer-encapsulated components were then broken out of the mold, the copper interconnect was wetted by the low-melting temperature solder, and the cubes were stirred in a 50 ºC bath of aqueous KBr and then cooled. The self-assembled structure was then immersed in methyl methacrylate (MMA) for 10 hours to dissolve the PMMA. MMA was used rather than chloroform because chloroform damaged the particular electronic components used in these experiments. After incorporating capacitors, LEDs, and a copper interconnect into the carrier structures, they were self-assembled and then actuated with a 10 $V_{pk\text{-}pk}$, 14 MHz signal. Figure 9A shows the working components: 2 capacitors, 2 LEDs, and 4 copper interconnect cubes arranged in a 2x2x2 array. The lead on the left is actuating a capacitor-encapsulated

cube, and the lead on the right is actuating a LED-encapsulated cube. The copper interconnect cubes enable 3D assembly and were fabricated by hand-wrapping copper tape around the PMMA cubes as in Figure 4. The 2x2x2 array was fabricated in a two step process. First, the four copper interconnect cubes were self-assembled to provide a seed layer for 3D growth. This seed layer was necessary because the LEDs and capacitors have only two leads. In previous experiments where only they were self-assembled, a one dimensional structure resulted: a line of LED and capacitor encapsulated cubes. After the 2D seed layer of copper interconnect was created, 2 LEDs and 2 capacitors were stirred into the bath, and they self-assembled on top of the interconnect, resulting in a 3D structure where the devices can be actuated in parallel and in selective combinations. The self-assembled structure was then immersed in MMA for 10 hours to dissolve the PMMA.

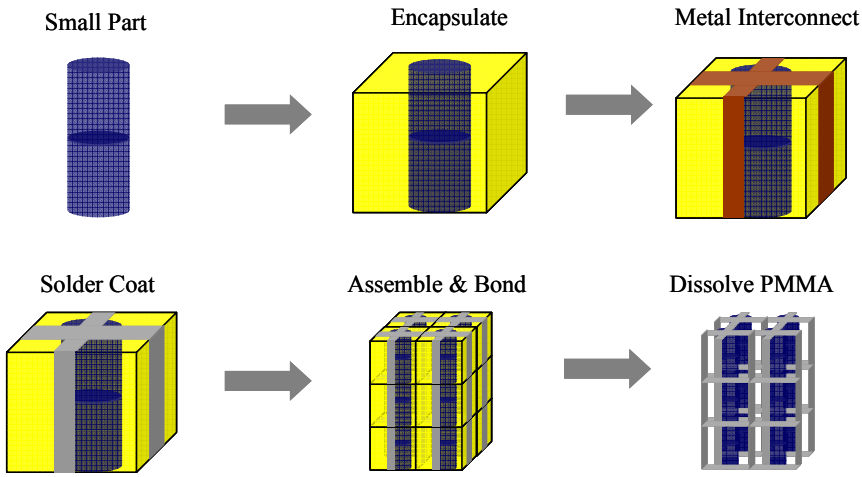

Figure 7. Small Part Encapsulated in Self-Assembly Carrier Structures and Subsequent Self-Assembly: A small part is encapsulated in polymer, the polymer is wrapped in copper tape to interconnect small parts, the copper tape is coated with low-melting temperature

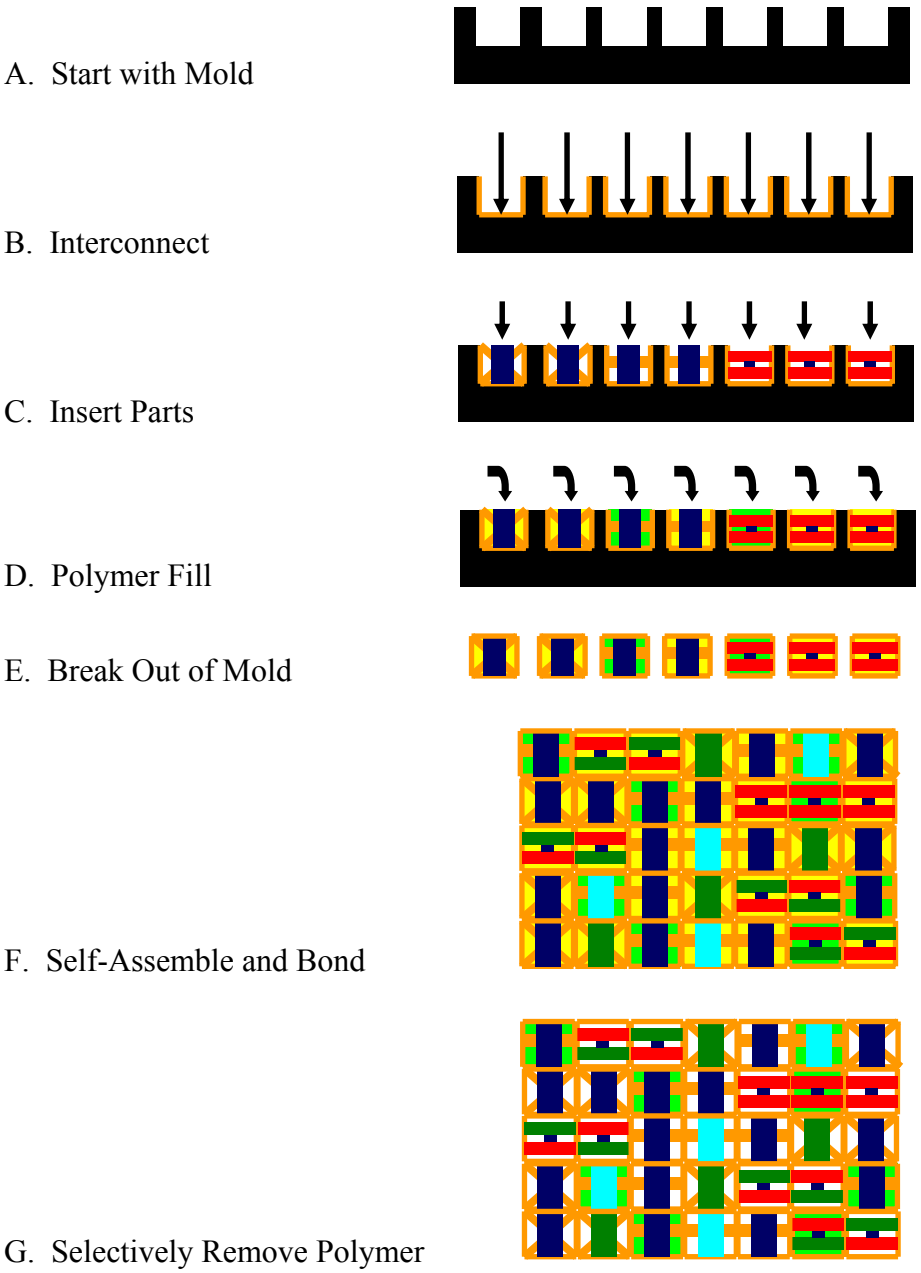

Figure 8. Manufacturing Strategy for Small Part Encapsulation and Self-Assembly: An interconnect is laid down in a mold. Small parts are inserted and soldered to the interconnect. Different polymers fill the mold, the structures are broken out, self-assembled & bonded, and the polymers can be selectively dissolved.

Figure 9B shows the actuated, PMMA-free capacitors, LEDs, and interconnect with an LED lit by a 10 $V_{pk\text{-}pk}$, 14 MHz signal. Dissolving the polymer matrix while maintaining the integrity of the electronics makes possible using MEMS devices with

moving parts such as mechanical actuators or resonators. Impedances of the circuit components increased after SA. Before SA, the copper tape had a resistance of 0.05 Ω, the LEDs had a resistance of 52 Ω, and the capacitors had an impedance of 10 Ω. After SA, the copper tape's resistance rose to 3 Ω, the LEDs' resistance rose to 54 Ω, and the capacitors' impedance rose to 150 Ω. The resistance and impedance increases are due to connection of electronic components with low-melting temperature alloy instead of standard solder and contact resistance at the interface of the carrier structures.

A. 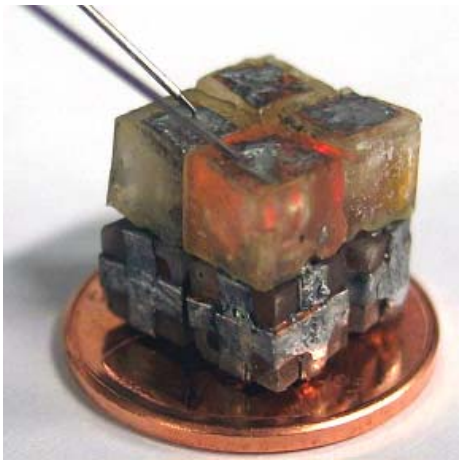 **B.** 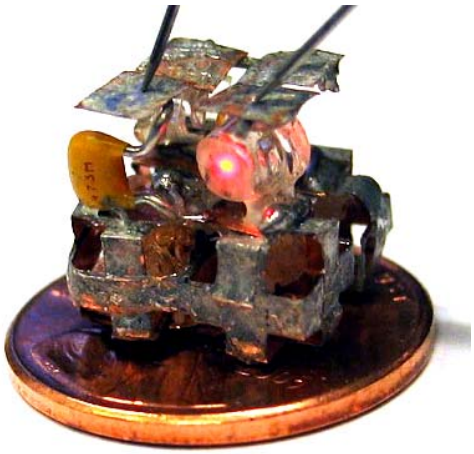

Figure 9. A) Electrically Actuated, Self-Assembled Capacitors and LEDs on a Penny (LED is lit). B) Methyl methacrylate (MMA) was used to dissolve PMMA from Electrically Actuated, Self-Assembled Capacitors and LEDs (LED on right is lit)

CHAPTER 3

MOLDING CERAMIC MICROSTRUCTURES ON FLAT AND CURVED SURFACES WITH AND WITHOUT EMBEDDED CARBON NANOTUBES

Alumina ceramic microstructures were micromolded from non-flexible and flexible molds. The flexible mold was used to fabricate mm-scale curved ceramic macrostructures with microstructures inside and outside of the curves. Patterned CNTs were transferred to ceramic, multilayered micropatterned CNT-ceramic electrical traces were fabricated, and CNT electrical traces were encapsulated with ceramic to inhibit oxidation.

3.1 Ceramic Microstructure Fabrication

The alumina ceramic used in this study was a commercially available low-shrinkage precursor (Cercanam by Ceramatec, Inc.), enabling high fidelity of mold features. The ceramic had a linear shrinkage less than 0.1% when cured below 800 ºC, 1-5% when cured at 1200 ºC, and 14-30% when cured at 1600 ºC. It had a maximum use temperature of 1600 ºC, density of 2.2 g/cm^3, 4-point room temperature flexural strength of 50 MPa, thermal conductivity of 0.2 - 5.0 W/m-K, and composition of greater than 95% alumina. The ceramic was first a slurry solution and could be molded or cast into features as small as 5 μm.

Three types of mold templates were used to fabricate microstructures as small as 5 μm on flat ceramic surfaces. These templates were etched silicon, embossed thermally decomposable polymer, and flexible PDMS. Figure 10 shows the process used for

molding ceramic to etched silicon. Ceramic precursor was vacuum molded into the master. The ceramic precursor was heated to 75 ºC for 2 hours to harden it into a green body, or a sample of uncured hardened ceramic precursor. The green body and silicon mold were then inserted into a Thermolyne 48000 box furnace and heated 450 ºC for 2 hours at a ramp rate of 5 ºC/sec. A razor blade removed the cured ceramic from the master. Figure 11 shows the resulting microstructures that were 50 µm wide and 5 µm tall. Deionized (DI) water diluted the precursor at a ratio of 2:1 (DI:Precursor) because the precursor was too viscous to vacuum mold in its original form. Although diluted precursor filled microstructures more easily than non-diluted precursor, it also shrank more than undiluted precursor as it dried into a green body, causing more cracks and lower fidelity replication of mold features.

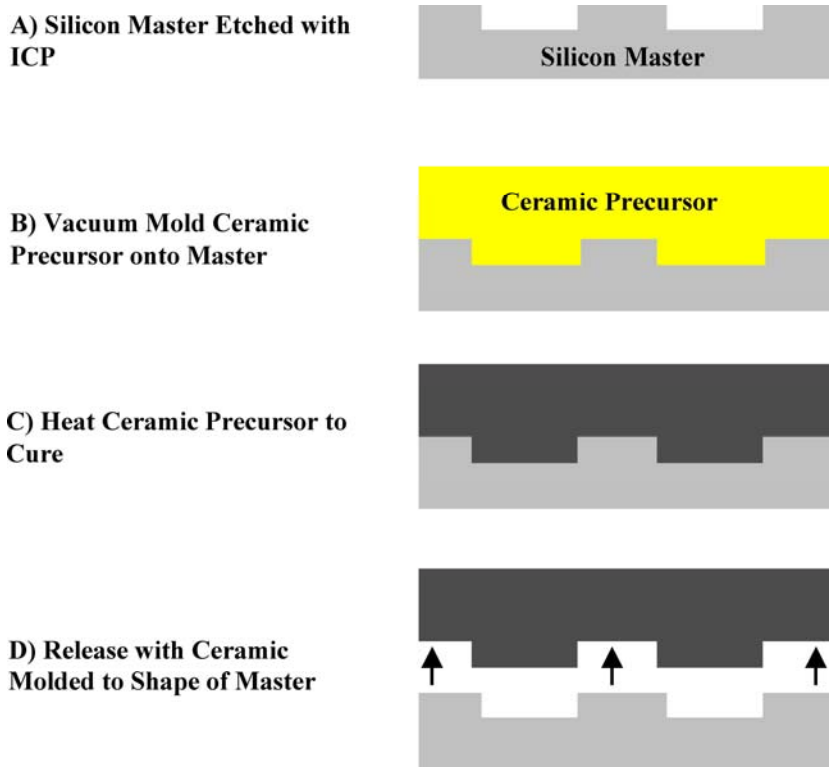

Figure 10. Process for micromolding ceramic micro structures on etched silicon: A) Begin with an etched silicon master. B) Vacuum mold ceramic precursor into the master

and heat ceramic precursor to 75 ºC for 2 hours to harden into green body. C) Heat the ceramic precursor to 450 ºC for 2 hours at a ramp rate of 5 ºC/sec. D) Remove the ceramic from the master.

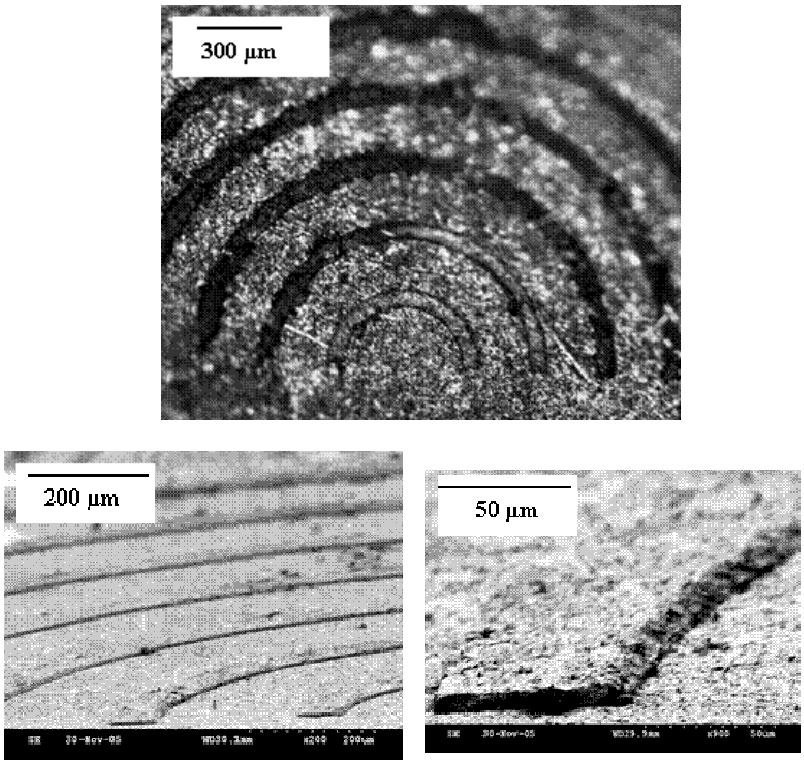

Figure 11. Ceramic microstructures molded from silicon

The second process for molding ceramic microstructures onto flat surfaces used embossed thermally decomposable polymer as a mold, shown in Figure 12. An etched silicon master with 5 µm features embossed the thermally decomposable polymer at room temperature with 22 MPa of pressure for 5 minutes. The silicon embossing tool was removed by sonication in water for one hour, and the diluted ceramic precursor was vacuum molded to the embossed thermally decomposable polymer. The assembly was heated to 75 ºC for 2 hours to harden the ceramic precursor into a green body. The assembly was then heated to 450 ºC for 4 hours at a ramp rate of 5 ºC/sec to cure the

ceramic and decompose the polymer. The assembly required an extra 2 hours of heating compared to the silicon-as-mold technique because the thermally decomposable polymer takes longer to decompose than the ceramic takes to cure. PUP version 2190 P [36] was used as the thermally decomposable polymer. PUP was spun onto a 100 mm silicon wafer at 1000 rpm with a 500 rpm/sec ramp rate for 30 seconds resulting in a 50 µm thick coating. The silicon embossing tool produced 1 µm deep indentions that are 5 µm wide, and Figure 13 shows the results of the ceramic molding.

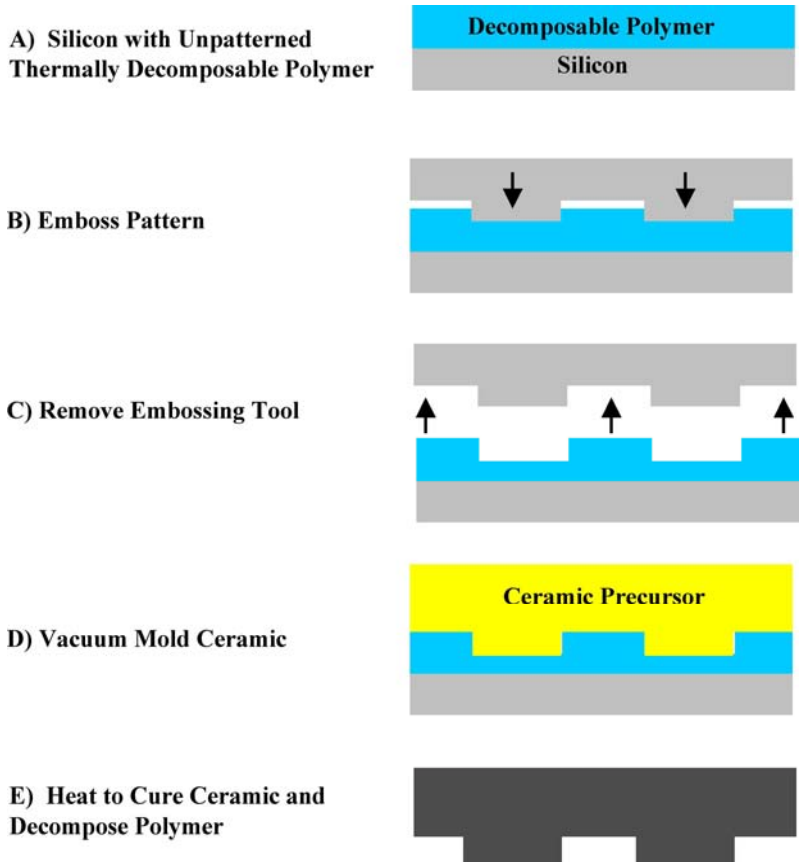

Figure 12. Process of Micropatterning thermally decomposable polymer via embossing and vacuum molding ceramic: A) Begin with unpatterned thermally decomposable polymer. B) Emboss a micropattern into the thermally decomposable polymer at room temperature with 22 MPa Pressure for 5 minutes. C) Remove the embossing tool. D) Vacuum mold ceramic precursor to the embossed thermally decomposable polymer and heat ceramic precursor to 75 ºC for 2 hours to harden into green body. E) Heat the

ceramic precursor to 450 ºC for 4 hours at a ramp rate of 5 ºC/sec to cure ceramic and decompose polymer.

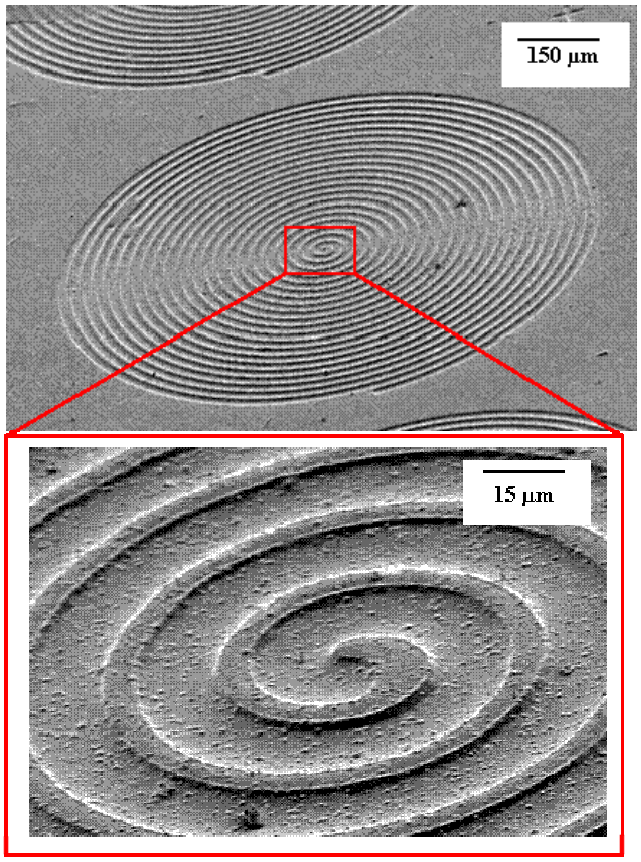

Figure 13. Microstructures transferred to ceramic via embossed thermally decomposable polymer

The third process for molding ceramic microstructures onto flat surfaces used flexible PDMS as a mold, shown in Figure 14. Beginning with a PDMS master molded from silicon, diluted ceramic precursor was vacuum molded into the master. The ceramic precursor was heated to 75 ºC for 2 hours to harden the precursor into a green body. Then the PDMS was peeled off the green body, and the green body was cured by heating to 450 ºC for 2 hours at a ramp rate of 5 ºC/sec. 5 µm features and features with an

aspect ratio of 2:1 were produced, shown in Figure 15. The flexibility and durability of PDMS molds enabled the fabrication of curved microstructured ceramic.

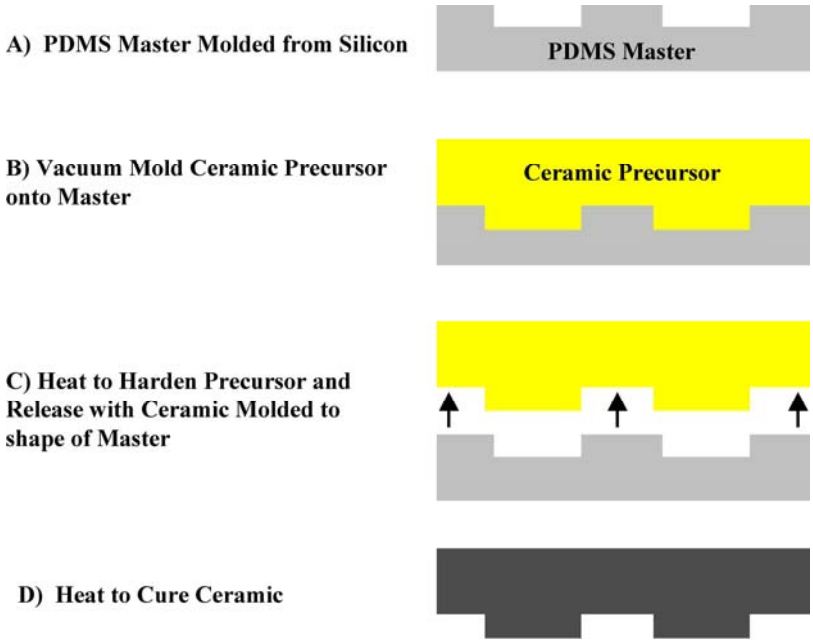

Figure 14. Process of micromolding ceramic structures with a PDMS mold: A) Begin with a PDMS master molded from silicon. B) Vacuum mold ceramic precursor into master. C) Heat ceramic precursor to 75 ºC for 2 hours to harden precursor into green body and then release green body from PDMS. D) Heat green body to 450 ºC for 2 hours at a ramp rate of 5 ºC/sec.

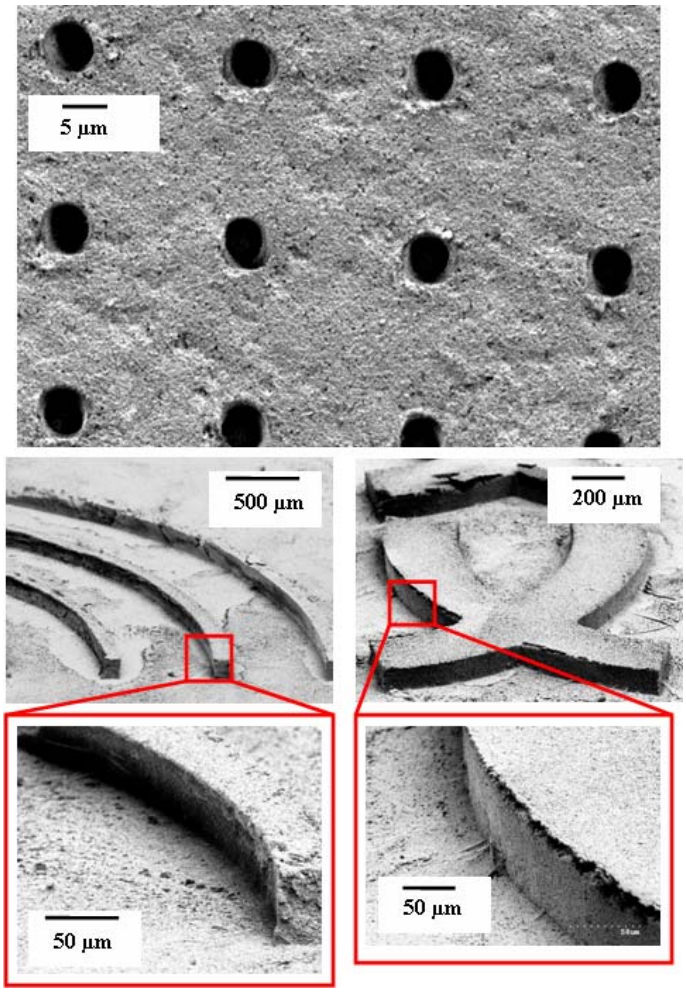

Figure 15. Microstructures molded into ceramic from PDMS

Molding ceramic with flexible PDMS micromolds in conjunction with curved macromolds produced microstructures as small as 20 µm inside and outside of curved surfaces. Figure 16 shows the process for making microstructures on the inside of a curved surface, and Figure 17 shows the process for making microstructures on the outside of a curved surface. The main difference between the "inside" and "outside" processes is that the PDMS mold is adhered to the outside of a curved macromold to produce ceramic microstructures on the inside of a curved surface, and the PDMS mold is placed in the inside of a curved mold to produce ceramic microstructures on the outside

of a curved surface. The ceramic precursor was heated to 75 ºC for 2 hours to harden the precursor into a green body. The green body was removed from the PDMS and heated to 450 ºC for 2 hours at a ramp rate of 5 ºC/sec in order to cure the ceramic. Figure 18 shows the resulting curved ceramic surface with microstructures on the inside of the curve**.** A macrostructure with a 3 mm radius of curvature was produced with 20 µm wide, 5 µm deep microstructures inside the curve. Figure 19 shows the resulting curved ceramic surface with microstructures on the outside of the curve. Using the process shown in Figure 19**,** a macrostructure with a 1.5 mm radius of curvature produced 200 µm wide, 50 µm deep microstructures.

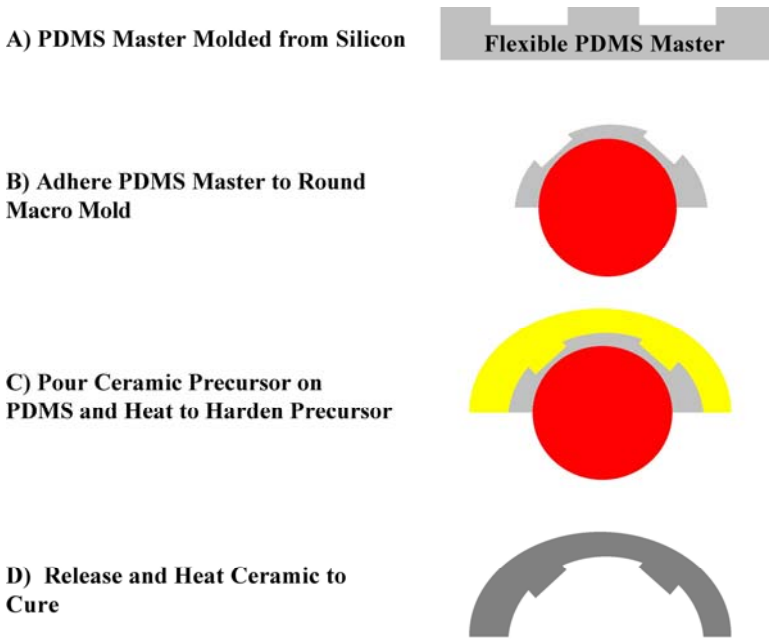

Figure 16. Process for molding curved ceramic with microstructures on inside of curve: A) Begin with a flexible PDMS master molded from silicon. B) Adhere PDMS master to round mold. C) Pour ceramic precursor onto PDMS and heat ceramic precursor to 75 ºC for 2 hours to harden precursor into green body. D) Release green body from PDMS and heat green body to 450 ºC for 2 hours at a ramp rate of 5 ºC/sec.

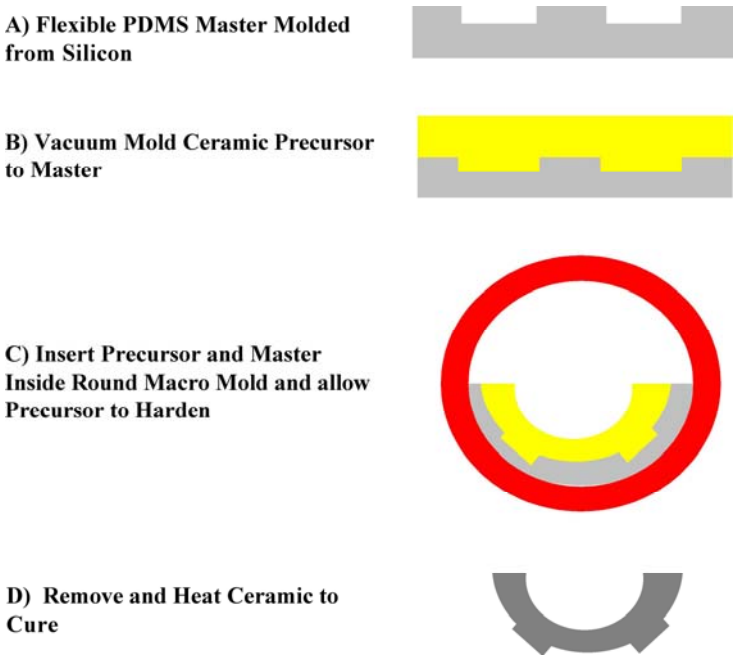

Figure 17. Process of molding microstructures on outside of curved surface. A) Begin with a flexible PDMS master molded from silicon. B) Vacuum mold ceramic precursor to PDMS master. C) Insert precursor and master into round mold and heat to 75 ºC for 2 hours to harden precursor into green body. D) Release green body from PDMS and heat green body to 450 ºC for 2 hours at a ramp rate of 5 ºC/sec.

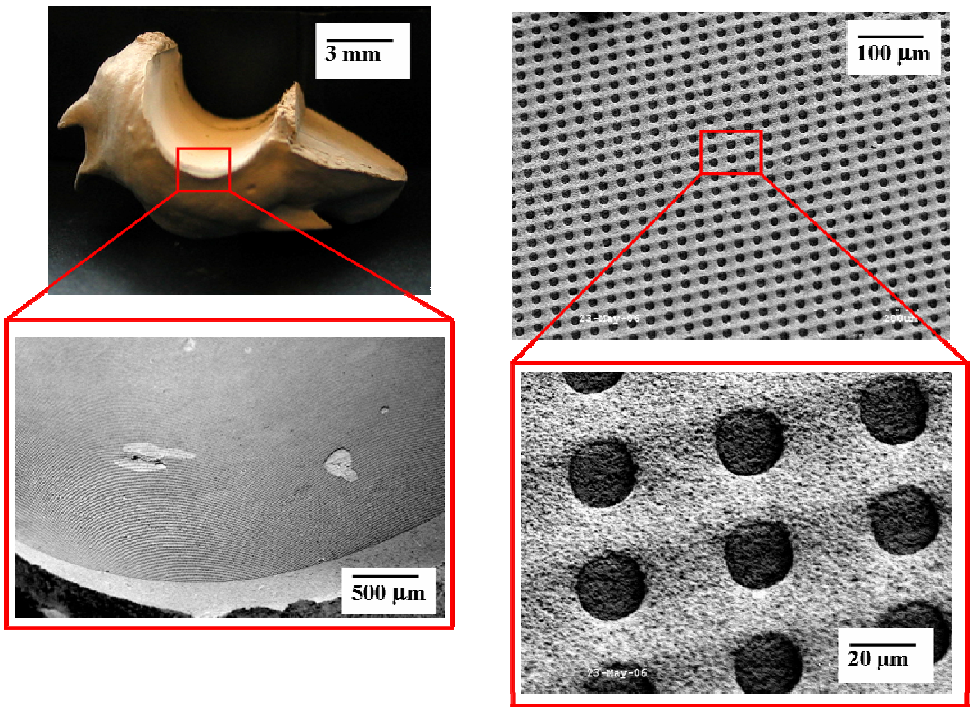

Figure 18. Microstructures molded inside ceramic with radius of curvature of 3 mm

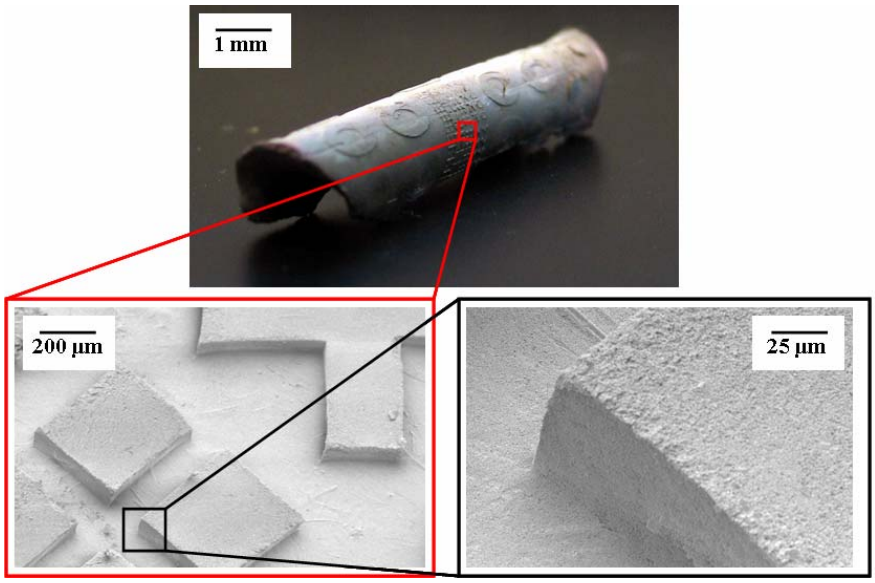

Figure 19. Microstructures molded on outside of curved ceramic with radius of curvature of 1.5 mm

3.2 Carbon Nanotube Integration

Ceramic precursor was vacuum molded to silicon micropatterned with CNTs, transferring electrically functional CNT micropatterns to ceramic. Multilayer CNT-ceramic devices were fabricated, increasing the density of CNT micropatterns and demonstrating a 3D micropatterning technique for CNTs on ceramics. Figure 20 shows the process for molding CNTs into ceramic. The CNTs were grown by depositing a 500 nm-thick coating of PECVD silicon dioxide onto a standard 100 mm silicon wafer. Next, a 10 nm-thick iron catalyst film was evaporated and micropatterned using photolithography and a lift-off technique. The iron catalyst was micropatterned in lines of 10 μm width, 8 mm length, and 200 μm pitch. The size and geometry of the catalyst micropattern can be controlled using standard microfabrication methods. To synthesize the CNTs, the micropatterned wafer was diced into 1 cm squares and placed into a high-temperature CVD growth furnace. The master templates were heated to 740 °C in nonreactive argon (500 sccm), then exposed to a mixture of acetylene (100 sccm), hydrogen (500 sccm), and methane (1000 sccm) for a growth period of 10 minutes followed by a cool down time of 2 hours to 100 °C and then to room temperature and ambient air. Multiwalled CNTs were produced that were 20 nm in diameter and 30-50 μm tall.

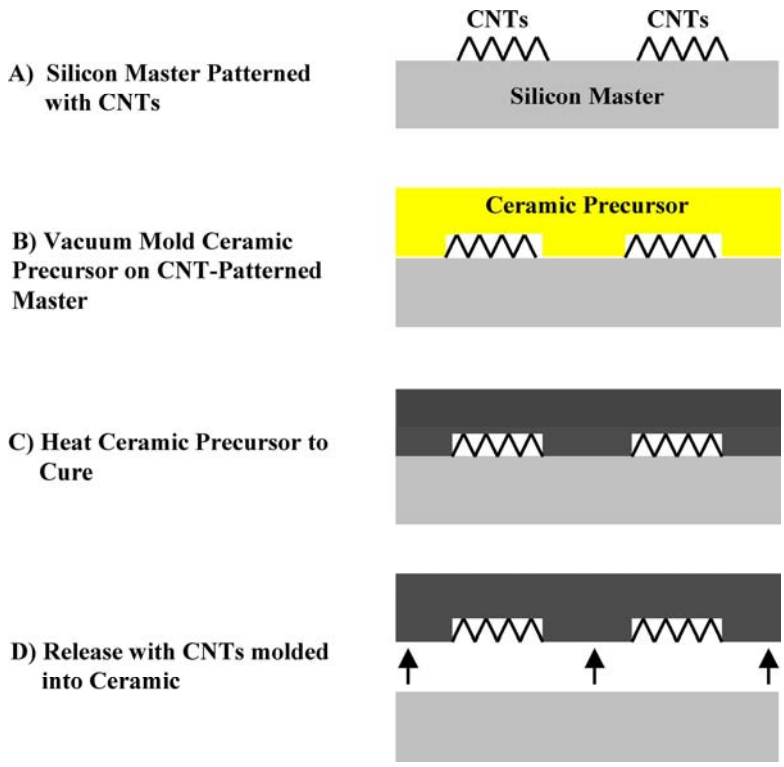

Figure 20. Process for Molding CNTs into Ceramic. A) Begin with silicon master micropatterned with CNTs. B) Vacuum mold ceramic precursor onto CNT-micropatterned master and heat to 75 ºC for 2 hours to harden precursor into green body. C) Heat green body to 450 ºC for 2 hours at a ramp rate of 5 ºC/sec. D) Release ceramic with transferred CNT micropattern

The CNT transfer process began with a silicon-silicon oxide master micropatterned with CNTs. Diluted ceramic precursor was vacuum molded onto the CNT micropatterned master and heated to 75 ºC for 2 hours to harden the precursor into a green body. The assembly was heated to 450 ºC for 2 hours at a ramp rate of 5 ºC/sec to cure the ceramic with CNTs in it. A razor blade was used to release the ceramic from the silicon with the CNT micropattern transferred. Figure 21 shows the results of the transfer where CNTs integrated into the porous ceramic are clearly seen. Titanium/Gold electrical bond pads, with 10 nm-thick Titanium and 200 nm-thick Gold, were evaporated onto only the ends of the CNT traces to test the electrical characteristics of the CNT-

ceramic device. Figure 22 shows the electrical characteristics of two samples that were fabricated under identical conditions. Both samples showed good linear I-V characteristics. Sample 1 had a resistance of 0.69 kΩ while Sample 2 had a resistance of 0.85 kΩ. The electrical characterization graphs will be revisited in the following section on oxidation inhibition. Figure 23 shows the process used to fabricate multilayer CNT-ceramic devices. Ceramic precursor was vacuum molded onto a CNT-micropatterned master, and a 2nd micropatterned master was placed onto the wet ceramic precursor. The assembly was heated to 75 ºC for 2 hours to harden the precursor into a green body, and the assembly was then heated to 450 ºC for 2 hours at a ramp rate of 5 ºC/sec. A razor blade released the ceramic leaving a double-sided micropatterned CNT-ceramic sample, shown in Figure 24.

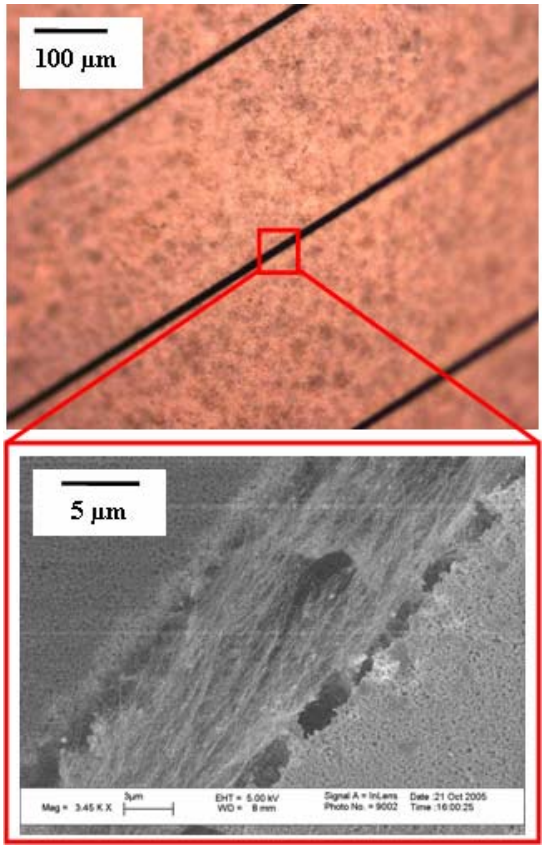

Figure 21. CNT traces transferred to Ceramic via vacuum-molding

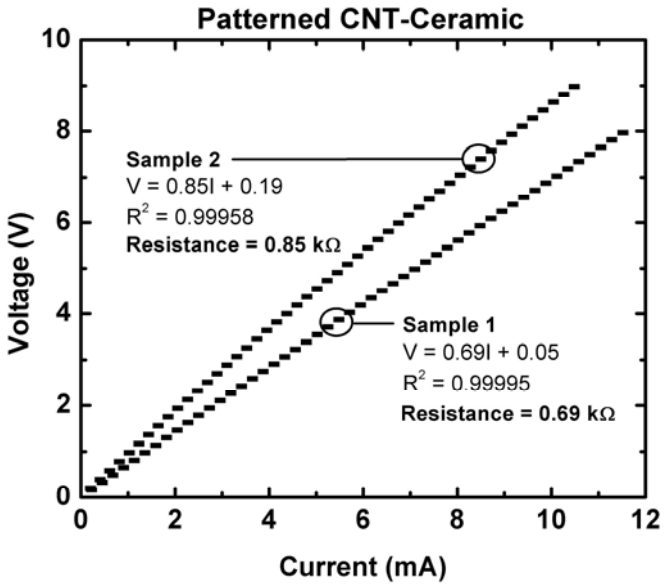

Figure 22. I-V Characteristics of Ceramic-CNT Samples 1 and 2

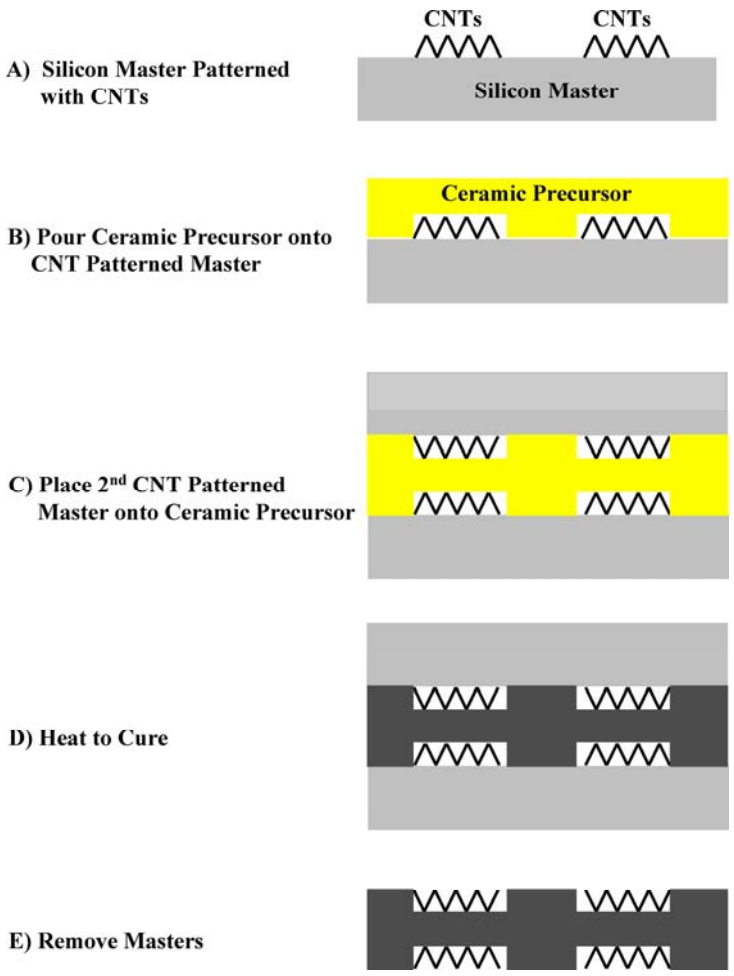

Figure 23. Process for molding CNT traces into multilayer devices: A) Begin with silicon master micropatterned with CNTs. B) Vacuum mold ceramic precursor onto CNT-micropatterned master. C) Place 2nd micropatterned master onto ceramic precursor and heat to 75 ºC for 2 hours to harden precursor into green body. D) Heat green body to 450 ºC for 2 hours at a ramp rate of 5 ºC/sec. E) Release ceramic with multiple transferred CNT micropatterns

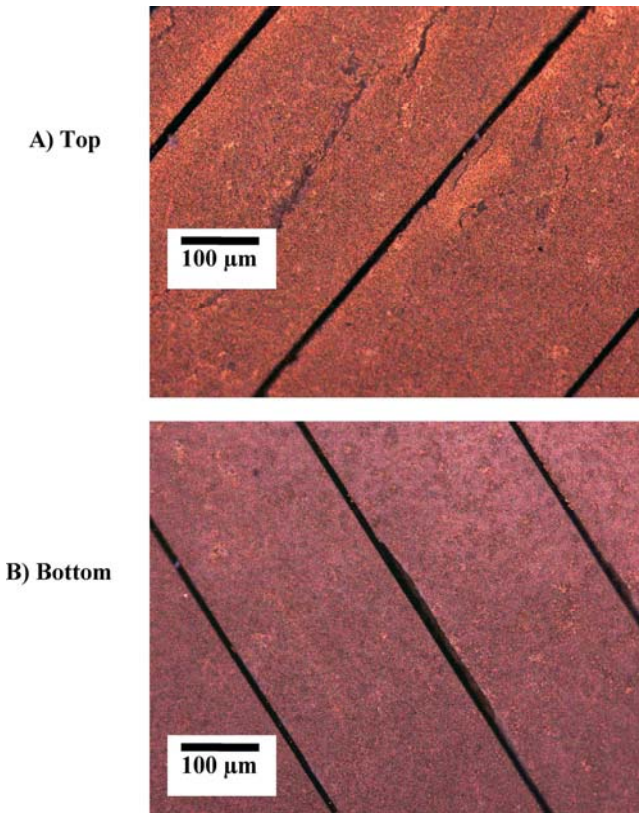

Figure 24. A) Top side of Multi-sided CNT-Ceramic Composite. B) Bottom side of Multi-sided CNT-Ceramic Composite

3.3 Oxidation Inhibition of carbon nanotubes

When the CNTs were transferred to the ceramic, they were exposed to the environment. When heated in air, the CNTs oxidize, and their properties can change. In order to protect the CNTs from oxidation, ceramic was used to encapsulate the CNTs, and a heating trial was performed to quantify the effectiveness of the encapsulant. Figure 25 shows the encapsulation process performed on Sample 1 whose electrical characteristics before encapsulation were displayed in Figure 22. Ceramic precursor was poured onto the CNT-ceramic device. A shadow mask prevented the ceramic precursor

from covering the Titanium/Gold electrical pads so that electrical characterization could be performed later. The assembly was heated to 75 ºC for 2 hours to harden the ceramic precursor into a green body. The shadow mask was then removed, exposing the Titanium/Gold electrical pads, and the encapsulated CNT-ceramic device was heated to 450 ºC for 2 hours at a ramp rate of 5 ºC/sec to cure the encapsulant ceramic. The encapsulated sample was then placed in a Thermolyne 59300 tube furnace along with the non-encapsulated Sample 2 whose electrical characteristics were shown in Figure 22. The encapsulated and non-encapsulated samples were heated to 700 ºC for 1 minute at a temperature ramp of 35 ºC/sec. They were then cooled to room temperature over 20 minutes, and electrical characterization was performed again to determine how well the ceramic encapsulant on Sample 1 protected the CNTs from oxidation. Figure 26 shows the post-oxidation electrical characteristics of the encapsulated Sample 1 and the post-oxidation electrical characteristics of the non-encapsulated Sample 2. While the resistance of the encapsulated sample increased by 43%, the resistance of the non-encapsulated sample increased by 105%. The ceramic encapsulant partially protected the CNTs from the effects of oxidation. This oxidation protection process could allow the benefits of CNTs to be used in high temperature devices such as microreactors which are presently fabricated from ceramics.

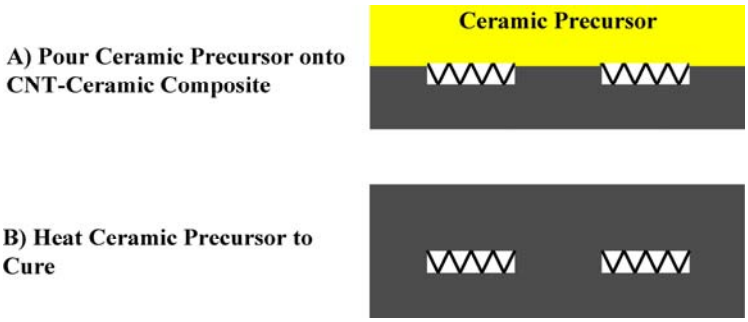

Figure 25. Process for fully embedding CNT traces in ceramic. A) Pour ceramic precursor onto CNT-ceramic composite and heat to 75 ºC for 2 hours to harden precursor into green body. B) Heat green body to 450 ºC for 2 hours at a ramp rate of 5 ºC/sec

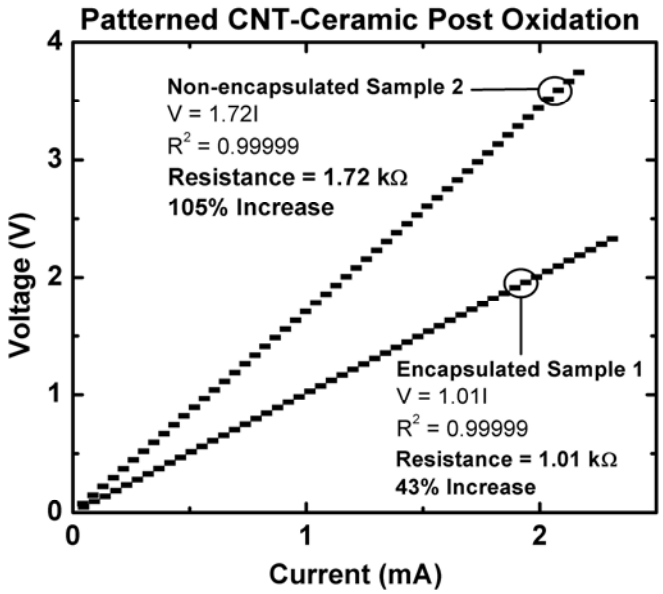

Figure 26. I-V Characteristics of Ceramic-CNT Sample 1 with CNTs fully embedded in ceramic and Sample 2 with CNTs not fully embedded in ceramic (exposed to the environment). Both samples were heated to 700 ºC for one minute. The electrical resistance of Sample 1 increased by 43%, and the electrical resistance of sample 2 increased by 105%.

CHAPTER 4

CONCLUSIONS AND FUTURE WORK

4.1 Conclusions

In this study, the main objective was to develop new microfabrication techniques using polymers in order to benefit from their low cost and high processing flexibility. PMMA was used as a sacrificial carrier material for the SA of heterogeneous devices in 3D. Encasing the heterogeneous devices in PMMA in such a way that resulted in similar structures made it possible to interconnect them without the concern of what devices were being interconnected. Using PMMA as a sacrificial material in this way allowed the self-assembly of any set of devices regardless of shape or function. Embossed thermally decomposable polymer was also used as a micromold for ceramic with features of 5 μm, enabling ceramic micromolding to benefit from the low cost, high throughput nature of embossing. Flexible PDMS was used as a curved ceramic micromold, and microfeatures were created on the inside and outside of the curves. The use of curved macromolds containing microfeatures can lead to devices such as microfluidic dissipators for gas and fluid dispersion.

4.2 Future Work on Self-Assembly

In the future, a larger variety of components will be cast into the SA carrier structures: batteries, transmitters, receivers, sensors, and digital & analog electronics. Component casting techniques will expand SA's toolbox of useable functional devices

and take advantage of the 3D range SA provides. The use of multi-lead devices will take advantage of more than two sides of the carrier structures. Smaller components and molds will be used to increase system function density.

To become a more powerful manufacturing technique, Selective SA will need to be achieved. SA is selective when specific surfaces are directed to mate with other specific surfaces. Selective SA would enable the manufacture of devices comprised of heterogeneous components where a specific order of the components is necessary. One possible path to selective SA is the use of a density-stratified solution. The stratification could provide a way for structures of different densities to self-assemble separately and be combined later. Using a variety of polymers with different densities could provide a simple route to making structures of different densities while enabling selective dissolution of the carrier material. Another possible path to selective SA is molding alignment features like those described previously [24] into the SA carrier structures. Proper use of these features should cause carrier structures to accept or reject other carrier structures by design.

4.3 Future Work on Ceramic Micromolding and Nanomaterial Transfer

Methods will be developed to combine the molding of microstructures with the transfer of nanomaterial. Etched silicon with CNT micropatterns could be a mold for such a combination, or embossing the features and CNTs into PMMA could provide a sacrificial mold. A more detailed study will be conducted on the inhibition of oxidation of CNTs through ceramic encapsulation by experimenting with precursor hardening

times, precursor dilution, and smaller ceramic particulates to improve the exclusion of air.

REFERENCES

1. Liew L.-A., W. Zhang, L. An, S. Shah, R. Lou, Y. Liu, T. Cross, M.L. Dunn, V. Bright, J.W. Daily, R. Raj, and K. Anseth 2001 *New Materials, Innovative Processing and Future Applications* American Ceramic Society Bulletin. **80**(5): p. 25.

2. Morales A.M., R. Pitchumani, T.J. Garino, A.K. Gutmann, and L.A. Domeier 2005 *Fabrication of Ceramic Microstructures via Microcasting of Nanoparticulate Slurry* Journal of American Ceramics Society. **88**(3): p. 570-578.

3. Tummala R.R., E.J. Rymaszewski, and A.G. Klopfenstein, *Microelectronics Packaging Handbook: Semiconductor Packaging Part II*. 2nd ed. 1997, Boston: Kluwer Academic Publishers. 156-160.

4. Yang H., P. Deschatelets, S.T. Brittain, and G.M. Whitesides 2001 *Fabrication of High Performance Ceramic Microstructures from a Polymeric Precursor Using Soft Lithography* Advanced Materials. **13**(1): p. 54-58.

5. Monajemi P., P.J. Joseph, P.A. Kohl, and F. Ayazi 2005 *A Low Cost Wafer-Level MEMS Packaging Technology* IEEE: p. 634-637.

6. Rowland H.D. and W.P. King 2004 *Polymer deformation and filling modes during microembossing* Journal of Micromechanics and Microengineering. **14**: p. 1625–1632.

7. Rowland H.D., A.C. Sun, P.R. Schunk, and W.P. King 2005 *Impact of polymer film thickness and cavity size on polymer flow during embossing: toward process design rules for nanoimprint lithography* Journal of Micromechanics and Microengineering. **15**: p. 2414-2425.

8. Cannon A.H., Y. Hua, C.L. Henderson, and W.P. King 2005 *Self-assembly for three-dimensional integration of functional electrical components* Journal of Micromechanics and Microengineering. **15**: p. 2172–2178.

9. Clark T.D., R. Ferrigno, J. Tien, K.E. Paul, and G.M. Whitesides 2002 *Template-Directed Self-Assembly of 10 um Sized Hexagonal Plates* Journal of the American Chemical Society. **124**: p. 5419-5426.

10. Corporation A.T., *Alien Technology Corporation 1999 Fluidic Self-Assembly White Paper* www.alientechnology.com/ accessed 08/2006.

11. Martin B.R., D.C. Furnange, T.N. Jackson, T.E. Mallouk, and T.S. Mayer 2001 *Self-Alignment of Patterned Wafers Using Capillary Forces at a Water-Air Interface* Adv. Funct. Mater. **11**(5): p. 381-386.

12. Whitesides G.M. and B. Grzybowski 2002 *Self-Assembly At All Scales* Science. **295**: p. 2418-2421.

13. Xiong X., Y. Hanein, J. Fang, Y. Wang, W. Wang, D.T. Schwartz, and K.F. Böhringer 2003 *Controlled Multibatch Self-Assembly of Microdevices* JMEMS. **12**(2): p. 117-127.

14. Srinivasan U., D. Liepmann, and R.T. Howe 2001 *Microstructure to Substrate Self-Assembly Using Capillary Forces* JMEMS. **10**(1): p. 17-24.

15. Gracias D.H., J. Tien, T.L. Breen, C. Hsu, and G.M. Whitesides 2000 *Forming Electrical Networks in Three Dimensions by Self-Assembly* Science. **289**: p. 1170-1172.

16. Grzybowski B., H.A. Stone, and G.M. Whitesides 2000 *Dynamic Self-Assembly of Magnetized Millimetre-Sized Objects Rotating at a Liquid-Air Interface* Nature. **405**: p. 1033-1036.

17. Gracias D.H., V. Kavthekar, J.C. Love, K.E. Paul, and G.M. Whitesides 2002 *Fabrication of Micrometer-Scale, Patterned Polyhedra by Self-Assembly* Adv. Mater. **14**(3): p. 235-238.

18. Syms R.R.A., E.M. Yeatman, V.M. Bright, and G.M. Whitesides 2003 *Surface Tension-Powered Self-Assembly of Microstructures—The State-of-the-Art* JMEMS. **12**(4): p. 387-417.

19. Bowden N., A. Terfort, J. Carbeck, and G.M. Whitesides 1997 *Self-Assembly of Mesoscale Objects into Ordered Two-Dimensional Arrays* Science. **276**(11): p. 233-235.

20. Madou M.J., *Fundamentals of Microfabrication: The Science of Miniaturization*. 2nd ed. 2002: CRC Press. 452-453.

21. Srinivasan U., Liepmann, D. and Howe, R. T. 2001 *Microstructure to Substrate Self-Assembly Using Capillary Forces* JMEMS. **10**(1): p. 17-24.

22. Jacobs H.O., A.R. Tao, A. Schwartz, D.H. Gracias, and G.M. Whitesides 2002 *Fabrication of Cylindrical Display by Patterned Assembly* Science. **296**(5566): p. 323-325.

23. Böhringer K.F. 2003 *Surface modification and modulation in microstructures: controlling protein adsorption, monolayer desorption and micro-self-assembly* Journal of Micromechanics and Microengineering. **13**: p. S1-S10.

24. Böhringer K.F., U. Srinivasan, and R.T. Howe. *Modeling of Capillary Forces and Binding Sites for Fluidic Self-Assembly*. in *14th IEEE International Conference MEMS 2001*. 2001.

25. Greiner A., J. Lienemann, J.G. Korvink, X. Xiong, Y. Hanein, and K.F. Böhringer. *Capillary Forces in Micro-Fluidic Self-Assembly*. in *Fifth International Conference on Modeling and Simulation of Microsystems (MSM'02)*. San Juan, Puerto Rico, USA.

26. Fang J. and K.F. Böhringer 2005 *High Yield Batch Packaging of Micro Devices With Uniquely Orienting Self-Assembly* 18th IEEE International Conference on Micro Electro Mechanical Systems, Miami, FL: p. 12-15.

27. Liang S.-H., K. Wang, and K.F. Böhringer. *Self-Assembly of MEMS Components in Air Assisted by Diaphragm Agitation*. in *18th IEEE International Conference on Micro Electro Mechanical Systems, Miami, FL*. 2005.

28. Kladitis P.E., V.M. Bright, and J.P. Kharoufeh 2004 *Uncertainty in Manufacture and Assembly of Multiple-Joint Solder Self-Assembled Microelectromechanical Systems (MEMS)* Journal of Manufacturing Processes. **6**(1): p. 32-50.

29. Breen T.L., J. Tien, S.R.J. Oliver, T. Hadzic, and G.M. Whitesides 1999 *Design and Self-Assembly of Open, Regular, 3D Microstructures* Science. **284**: p. 948-951.

30. Zheng W., P. Buhlmann, and H.O. Jacobs 2004 *Sequential shape-and-solder-directed self-assembly of functional microsystems* Proceedings of the National Academy of Sciences of the United States of America. **101**(35): p. 12814-12817.

31. Zheng W., J. Chung, and H.O. Jacobs 2005 *Non-Robotic Fabrication of Packaged Microsystems by Shape-and-Solder Directed Self-Assembly* 18th IEEE International Conference on Micro Electro Mechanical Systems, Miami, FL: p. 8-11.

32. Zheng W. and H. Jacobs 2004 *Shape-and-solder-directed self-assembly to package semiconductor device segments* Applied Physics Letters. **85**(16): p. 3635-3637.

33. Zheng W. and H. Jacobs 2005 *Fabrication of multicomponent microsystems by directed three-dimensional self-assembly* Advanced Functional Materials. **15**(5): p. 732-738.

34. Knitter R., D. Gohring, P. Risthaus, and J. Hausselt 2001 *Microfabrication of ceramic microreactors* Microsystem Technologies. **7**: p. 85-90.

35. Heule M., J. Schell, and L.J. Gauckler 2003 *Powder-Based Tin Oxide Microcomponents on Silicon Substrates Fabricated by Micromolding in Capillaries* Journal of American Ceramics Society. **86**(3): p. 407-412.

36. Heule M. and L.J. Gauckler 2001 *Gas Sensors Fabricated from Ceramic Suspensions by Micromolding in Capillaries* Advanced Materials. **13**(23): p. 1790-1793.

37. Auger M.A., P.L. Schilardi, I. Caretti, O. Sanchez, G. Benitez, J.M. Albella, R. Gago, M. Fonticelli, L. Vazquez, R.C. Salvarezza, and O. Azzaroni 2005 *Molding and Replication of Ceramic Surfaces with Nanoscale Resolution* Small. **1**(3): p. 300-309.

38. Provin C., S. Monneret, H.L. Gall, and S. Corbel 2003 *Three-Dimensional Ceramic Microcomponents Made Using Microstereolithography* Advanced Materials. **15**(12): p. 994-997.

39. Heule M., S. Vuillemin, and L.J. Gauckler 2003 *Powder-Based Ceramic Meso- and Microscale Fabrication Processes* Advanced Materials. **15**(15): p. 1237-1245.

40. Treacy M.M.J., T.W. Ebbesen, and J.M. Gibson 1996 *Exceptionally high Young's modulus observed for individual carbon nanotubes* Nature. **381**: p. 678-680.

41. Ebbesen T.W., H.J. Lezec, H. Hiura, J.W. Bennett, H.F. Ghaemi, and T. Thio 1996 *Electrical conductivity of individual carbon nanotubes* Nature. **382**.

42. Iijima S. 1991 *Helical microtubules of graphitic carbon* Nature. **354**: p. 56-58.

43. Heer W.A.d., A. Chatelain, and D. Ugarte 1995 *A Carbon Nanotube Field-Emission Electron Source* Science. **270**(5239): p. 1179-1180.

44. Park S.-J., J.G. Eden, and K.-H. Park 2004 *Carbon nanotube-enhanced performance of microplasma devices* Applied Physics Letters. **84**(22).

45. Cui J.B., R. Sordan, M. Burghard, and K. Kern 2002 *Carbon nanotube memory devices of high charge storage stability* Applied Physics Letters. **81**(17): p. 3260-3262.

46. Kang S., J.P. Johnston, T. Arima, and F.B. Printz, *Microscale Radial-Flow Compressor Impeller Made of Silion Nitride: Manufacturing and Performance*, in *Transactions of the ASME*. 2004. p. 358-365.

47. Ahn S.-J. and J. Moon 2005 *Vacuum-Assisted Microfluidic Lithography of Ceramic Microstructures* Journal of American Ceramics Society. **88**(5): p. 1171-1174.

48. Epstein A.H. 2004 *Millimeter-Scale, Micro-Electro-Mechanical Systems Gas Turbine Engines* Journal of Engineering for Gas Turbines and Power. **126**: p. 205-226.

49. Cooper A.G., S. Kanga, J.W. Kietzmana, F.B. Prinza, J.L. Lombardi, and L.E. Weiss 1999 *Automated fabrication of complex molded parts using Mold Shape Deposition Manufacturing* Materials and Design. **20**: p. 83-89.

50. Henderson C.L., W.P. King, C.E. White, and H.R. Rowland. *Microsystems Manufacturing via Embossing of Thermally Sacrificial Polymers*. in *Materials Research Society Symposium Proceedings*. 2004.

51. Rowland H.D., W.P. King, A.C. Sun, and P.R. Schunk 2005 *Simulations of nonuniform embossing: The effect of asymmetric neighbor cavities on polymer flow during nanoimprint lithography* Journal of Vacuum Science Technology B. **23**(6): p. 2958-2962.

52. Choi E.S., J.S. Brooks, D.L. Eaton, M.S. Al-Haik, M.Y. Hussaini, H. Garmestani, D. Li, and K. Dahmen 2003 *Enhancement of thermal and electrical properties of carbon nanotube polymer composites by magnetic field processing* Journal of Applied Physics. **94**(9): p. 6034-6039.

53. Allen A.C., E.O. Sunden, A.H. Cannon, S. Graham, and W.P. King 2006 *Nanomaterial transfer using hot embossing for flexible electronic devices* Virtual Journal of Nanoscale Science and Technology. **13**(9).

54. Kim Y.A., T. Hayashi, M. Endo, Y. Gotoh, N. Wada, and J. Seiyama 2006 *Fabrication of aligned carbon nanotube-filled rubber composite* Scripta Materialia. **54**: p. 31-35.

55. Allen A.C., E. Sunden, A. Cannon, S. Graham, and W. King 2006 *Nanomaterial transfer using hot embossing for flexible electronic devices* Applied Physics Letters. **88**(083112): p. 1-3.

56. Haberecht J., F. Krumeich, M. Stalder, and R. Nesper 2005 *Carbon nanostructures on high-temperature ceramics – a novel composite material and its functionalization* Catalysis Today. **102**(103): p. 40-44.

57. Jung Y.J., S. Kar, S. Talapatra, C. Soldano, G. Viswanathan, X. Li, Z. Yao, F.S. Ou, A. Avadhanula, R. Vajtai, S. Curran, O. Nalamasu, and P.M. Ajayan 2006 *Aligned Carbon Nanotube-Polymer Hybrid Architectures for Diverse Flexible Electronic Applications* Nano Letters. **6**(3): p. 413-418.

58. Peigney A. 2003 *Tougher ceramics with nanotubes* Nature Materials. **2**: p. 15-16.

59. Zhan G.-D., J.D. Kuntz, J. Wan, and A.K. Mukherjee 2002 *Single-wall carbon nanotubes as attractive toughening agents in alumina based nanocomposites* Nature Materials. **2**: p. 38-42.

60. Zhan G.-D., J.D. Kuntz, A.K. Mukherjee, P. Zhu, and K. Koumoto 2006 *Thermoelectric properties of carbon nanotube/ceramic nanocomposites* Scripta Materialia. **54**: p. 77-82.

61. Cha S.I., K.T. Kim, K.H. Lee, C.B. Mo, and S.H. Hong 2005 *Strengthening and toughening of carbon nanotube reinforced alumina nanocomposite fabricated by molecular level mixing process* Scripta Materialia. **53**: p. 793-797.

62. Lim S.C., C.S. Jo, H.J. Jeong, Y.M. Shin, Y.H. Lee, I.A. Samayoa, and J. Choi 2002 *Effect of Oxidation on Electronic and Geometric Properties of Carbon Nanotubes* Japan Journal of Applied Physics Letters. **41**(9): p. 5635-5639.

63. Metspec #117 from MCP Alloys www.mcp-group.com acessed 08/2006.